Research Square

Preprints are preliminary reports that have not undergone peer review.
They should not be considered conclusive, used to inform clinical practice,
or referenced by the media as validated information.

Cutting performance and antifriction mechanism of Al2O3/TiC/TiB2/h-BN@Al2O3 self-lubricating ceramic tool

Yuxin Shi
Guangchun Xiao
Zhaoqiang Chen (czq@qlu.edu.cn)
Qilu University of Technology (Shandong Academy of Sciences) https://orcid.org/0000-0003-3380-3689
Lianggang Ji
Mingdong Yi
Jingjie Zhang
Hui Chen
Chonghai Xu

Research Article

Keywords: Ceramic tool, Cutting performance, Wear mechanism, Self-healing, Self-lubricating

Posted Date: March 24th, 2022

DOI: https://doi.org/10.21203/rs.3.rs-1460799/v1

License: This work is licensed under a Creative Commons Attribution 4.0 International License.
Read Full License

Version of Record: A version of this preprint was published at The International Journal of Advanced Manufacturing Technology on January 3rd, 2023. See the published version at https://doi.org/10.1007/s00170-022-10734-x.

Abstract

The machinability and wear reduction mechanism of self-repairing and self-lubricating ceramic tools sintered by vacuum hot-pressing method in the dry turning of 40Cr hardened steel were studied. By comparing the cutting performance and wear morphology of AT (Al_2O_3/TiC) ceramic tools under different cutting parameters, it was found that AT10B@5 (Al_2O_3/TiC/10 vol% TiB_2/5 vol%h-BN@Al_2O_3) tool has a longer service life and better machining quality. Owing to the precipitation of solid lubricant during the cutting of AT10B@5 ceramic tool, the friction force during the cutting is reduced, thus decreasing the cutting force and cutting temperature of AT10B@5 ceramic tool during the cutting. The main cutting force decreased by 20.8%; the cutting temperature decreased by 22.2%; and the friction coefficient of front tool face decreased by 11.6% compared with AT tool. This effectively improved the surface quality of working parts, reduced the tool wear, increased the processing quality of work piece, and prolonged the tool life.

Introduction

Dry cutting [1, 2, 3], a new processing technology that can effectively reduce environmental pollution, has been widely studied in the world. However, in the processing of difficult-to-process materials, because of the low thermal conductivity of the difficult-to-process material itself, it is difficult to remove cutting heat through the chip, and dry cutting tool and work piece will have higher friction and adhesion, making the cutting temperature very high, aggravating tool wear, and shortening the life of the tool. Therefore, the manufacturing of new cutting ceramic tools that satisfy the processing conditions and effectively reduce the friction and increase the life has become the research focus.

A large number of scholars studied the wear resistance of new ceramic tools. Huang et al. [4, 5] prepared ceramic tools with high bending strength and fracture toughness using the SiC whisker toughening method, resulting in a higher cutting wear resistance, but still could not solve the problems of high friction and high cutting temperature in dry cutting. Deng et al. [6] conducted dry high-speed machining experiments on hardened steel using Al_2O_3/ TiB_2-based ceramic tools and found that an increase in cutting temperature resulted in the formation of a self-lubricating oxide film on the tool-chip interface. The lubrication film reduced the bonding effect between the tool and working parts, and between the tool and chip, thus reducing the tool wear and improving the tool life. He et al. [7] studied the wear morphology of high hardness alloy steel 20CrMo steel with coated cutting tool under dry cutting condition and pointed out that due to the good chemical stability and wear resistance of coating, the tool wear rate was greatly reduced. Xing et al. [8] added solid lubricant to Al_2O_3/TiC-based ceramic tools. The cutting force, cutting temperature, friction coefficient, and tool wear of the self-lubricating tool substantially reduced compared with those of a traditional tool, thus effectively improving the cutting performance of traditional Al_2O_3/TiC ceramic tool, and it is suitable for the stable dry cutting of hardened steel. Deng et al. [9] determined that the mechanism was the formation of self-lubricating film on the tool-chip interface However, owing to the low performance of solid lubricants, traditional self-lubricating

ceramic tools have good wear reduction performance, but due to the low hardness, they cannot be applied well to cutting high-hardness working parts, limiting the promotion of the tool.

Considering the friction reduction and mechanical properties. SiC-coated h-BN powders ((h-BN)/SiC) [10] or Al_2O_3-coated h-BN powders ((h-BN)/Al_2O_3) [11] were used to substitute h-BN as solid lubricant. The cutting performance and wear resistance significantly improved compared with those of ceramic tools with direct lubricant, thus avoiding the adverse effects of direct addition of h-BN. Zhang et al. [12] used Al_2O_3-coated CaF_2 powders prepare ceramic tool materials to perform dry cutting experiments on 40Cr hardened steel. During processing, the CaF_2 precipitated from CaF_2@Al_2O_3 on the front of self-lubricating ceramic tool, and CaF_2@Al_2O_3 core-shell coated solid lubricant alleviated the adhesion of workpiece material on the tool, indicating that the addition of CaF_2@Al_2O_3 particle effectively reduced the adverse effect of directly adding CaF_2 particle on ceramic tool.

A ceramic tool is brittle [13, 14, 15]. During cutting, defect such as microcracks can easily occur. Thus, the mechanical properties of the tool are reduced. If not handled timely, the tool may even fail. Lange and Gupta [16] reported crack healing during heat treatment. Self-healing ceramic tools can effectively utilize the cutting heat, generate a liquid phase, fill cracks, and achieve self-healing of cracks. The self-healing of ceramic cracks [17, 18, 19]. can not only help to recover the material strength, but even improve the mechanical properties of the tool, important for improving the reliability of ceramic materials. Zhai et al. [20] studied the surface stress crack healing behavior of nickel oxide aluminum bronze (NAB)/Ti_3SiC_2 nanocrystalline composites that can simultaneously decompose and heal. Crack healing induced by wear was achieved by the decomposition and oxidation of Ti_3SiC_2 on the surface. The selective formation of SiO_2, TiO_2, and Al_2O_3 repaired the cracks during fretting wear. The formation of TiO_2 steadily decreased the friction torque. The improvement in friction performance was related to self-healing. Houjou et al. [21] studied the oxidation behavior of Si_3N_4/SiC composite ceramics as a function of temperature and time and the maximum surface crack size for complete healing. Huy and Makoto [22] studied SiC composite ceramics and found that surface crack closure can be attributed to the formation and volume expansion of oxidation product layer. Exothermic oxidation produces strong composites between the oxide formed and crack wall, which can effectively improve the performance of the material. However, oxide evaporation and gas formation are harmful to crack repair ability [23]. Nguyen et al. [24] studied the self-healing behavior and strength recovery of $YB_2Si_2O_7$-YB_2SiO_5-SiC ceramics reinforced by silicon carbide nanofillers and found that the main mechanism of crack healing is the silica glass filling crack and the YB_2SiO_7 volume expansion caused by the reaction of SiO_2 and Yb_2SiO_5. The cracks can be completely healed after heat treatment at 1250 ℃ for 5 h, and the bending strength of composite can be improved The problem of reducing the effect of self-healing ceramics by the volatilization of silica in reinforced materials was solved.

Wang et al. [25] prepared a Cu-MbT@HNTs/epoxy self-healing coating using epoxy resin and a Cu-MBT nanocomposite corrosion inhibitor. The Cu-MBT@HNTs/epoxy coating showed a higher polarization resistance and better self-healing properties than the blank epoxy coating and MBT@HNTs/epoxy

coating. This was due to the release of MBT inhibitor from HNTs under local alkaline conditions and the formation of an Fe-MBT inhibition film in the scratched area of steel matrix.

In this study, a new type of Al_2O_3/TiC/TiB_2/h-BN@Al_2O_3 self-lubricating ceramic tool with self-repairing ability was prepared using vacuum hot-pressing method. TiC is the reinforcing phase; TiB_2 is the repairing phase; and h-BN@Al_2O_3 is the lubricant. The cutting performance of the tool was studied by measuring the cutting force, cutting temperature, and surface roughness under different cutting parameters. The tool surface was characterized by scanning electron microscopy (SEM) and energy dispersive spectroscopy (EDS), and the wear mechanism and repair behavior of the tool during cutting were studied. This study is helpful to further show that the self-lubricating ceramic tool with self-healing function can obtain better surface machining quality when dry cutting 40Cr hardened steel.

Experimental

Preparation of ceramic tool

The raw materials required for the preparation of ceramic tools are shown in Table 1. Al_2O_3/TiC/10 vol%TiB_2/5 vol%h-BN@Al_2O_3, and Al_2O_3/TiC ceramic cutting tools were prepared using vacuum hot-pressing sintering. The sintering temperature was 1650°C; the holding time was 20 min; and the hot-pressing pressure was 32 MPa. The dry cutting tests of ceramic tools with TiB_2 particles and coated solid lubricant h-BN@Al_2O_3 particles were compared with those of Al_2O_3/TiC ceramic tools.

For the convenience of description, the ceramic tool with 10 vol%TiB_2 particles and 5 vol%h-BN@Al_2O_3 particles is denoted as AT10B@5, and the Al_2O_3/TiC ceramic tool is denoted as AT. Table 2shows the content and mechanical properties of the components in the tools.

Table 1
Raw materials for self-lubricating ceramic tool test with self-repairing ability

materials	grain size(μm)	manufacturers
Al_2O_3	0.5	Qinhuangdao Yinuo High-tech Material Development Co. LTD
TiC	0.5-1	Qinhuangdao Yinuo High-tech Material Development Co. LTD
TiB_2	1	Qinhuangdao Yinuo High-tech Material Development Co. LTD
MgO	0.5	Sinopharm Chemical Reagent Co. LTD
h-BN@Al_2O_3	0.2–0.5	Independently developed

Table 2. Distribution ratio and mechanical properties of self-lubricating ceramic tools with self-healing ability

materials	Content of each component（vol%）					Mechanical Properties		
	Al_2O_3	TiC	TiB_2	h-BN@ Al_2O_3	MgO	Flexural Strength (MPa)	Fracture Toughness ($MPa \cdot m^{1/2}$)	Vickers Hardness (GPa)
AT	69.65	29.85	0	0	0.5	624	5.2	17.9
ATB@5	59.15	25.35	10	5	0.5	610	5.17	17.89

Table 2 shows the mechanical properties of the two materials. The addition of h-BN@Al_2O_3 particles reduces the mechanical properties of the material. Compared with AT materials, the bending strength decreased by 2.24%, and the fracture toughness and Vickers hardness did not decrease.

The comprehensive mechanical properties of ceramic embryos prepared by vacuum hot-pressing sintering were tested. First, the material pretreatment including slicing, rough grinding, fine grinding, grinding, and polishing was conducted. The material was processed into standard strip samples with a surface roughness Ra of less than 0.1 μm and size of 3 mm × 4 mm × 35 mm. To eliminate the effect of stress concentration, each edge of the spline was chamfered. In this study, the flexural strength of ceramic tool samples was tested using a three-point flexural method. A WDW-50E microcomputer controlled electronic universal testing machine manufactured by Jinan Group Co., LTD. was used. An hV-120 Vickers hardness tester was used to measure the hardness of ceramic tool samples prepared using indentation method. In this study, the fracture toughness of ceramic materials was measured using indentation method. The elemental distribution of the material was analyzed by energy-dispersive X-ray spectroscopy (EDS).

Cutting experiment

The cutting workpiece was made of 40Cr hardened steel with a material hardness of 48–50 HRC.

Geometric parameters of ceramic tool: The tool size was 12.7 mm×12.7 mm×7.9 mm.

Table 3
Geometrical parameters of ceramic tools

Corner Radius γ_ε	Relief angle α_0	Inclination angle λ_S	Rake angle γ_0	Chamfering parameters $b_{r1} \times \gamma_{o1}$	Cutting edge angle κ_r
0.2mm	-5°	0°	-5°	0.1mm× -10°	45°

A CDE6140A lathe produced by Dalian Machine Tool Group was used as the machine tool, and the tool holder was Kenner GSSN R/L 2525M12-Mn7. The wear degree of the front and rear surface of the tool

was observed using a PXS-1020 tool microscope and SUPRATM 55 thermal field-emission scanning electron microscope. The tool failure standard was VB = 0.3 mm. When the tool failed, the total cutting distance was used as the basis for evaluating the cutting performance of the tool. The roughness of the workpiece surface was measured using a TR200 hand-held roughness meter. The cutting temperature was measured using a FLAR-A320 infrared thermal imager. The cutting force was measured using a Kistler 9129A dynamometer.

Results And Discussion

Cutting performance of tool

The effects of different cutting speeds (v), feed rates (f), and depths of cut (a_p) on the wear of tool material and the surface roughness of workpiece were studied to determine the cutting performance of ceramic tool in cutting 40Cr hardened steel.

Figure 1 shows the changes between the cutting distance S and (a) wear amount of back tool surface VB and (b) workpiece surface roughness Ra at different cutting speeds (f = 0.102 mm/r, a_p = 0.2 mm) when the AT10B@5 and AT tools cut the workpiece 40Cr hardened steel.

As shown in Fig. 1 (a), the cutting speed of the tool substantially affects the life of tool. When the cutting speed was 100 m/min, the effective cutting distance of AT10B@5 and AT tools was greater than 6000 m. The tool wear was small, and the wear rate was slow. With the increase in cutting speed, when the cutting speed increased to 300 m/min, the wear of back tool face increased rapidly with the increase in cutting distance, and the wear state of back tool face showed a linear growth state. When the effective cutting distance was about 5500 m, the wear state of back tool face reached the failure standard. The wear of back tool face of AT10B@5 tool showed a slow increasing trend, belonging to the stable wear state. The effective cutting distance was more than 6000 m, and the back tool face did not reach the wear state and can be continued to use. By comparing AT10B @ 5, similar knife surface wear rules can be found for the cutting tool. The effective cutting distance of AT10B @ 5 knives is longer compared with the AT tool, mainly because of the precipitation of a solid lubricant in high-speed cutting. This increased the lubrication effect of cutting tools, reduced the friction resistance between the cutting tool workpiece, and decreased the blade wear.

Figure 1 (b) shows that with the increase in the cutting speed of the two tools, the machining surface roughness of the workpiece had an overall downward trend. This shows that high-speed cutting can obtain better surface finishing quality. The surface roughness of workpiece after machining by AT tool was generally between 1 and 3.5. The surface roughness was large when the cutting speed was 100 m/min, and the surface roughness reached 3.3 when the cutting distance reached 6000 m. The workpiece surface roughness of AT10B@5 tool after machining was maintained in the range of 0.1–1. The overall surface roughness was reduced compared with AT tool. Under the same cutting conditions, the surface roughness of AT10B@5 tool was smaller. This is because the addition of h-BN@Al_2O_3 substantially

increased the lubrication performance of the tool. During cutting, the solid lubricant h-BN@Al_2O_3 precipitated on the surface of the tool and dragged to form a film, thus reducing the friction between the tool and workpiece and improving the workpiece surface processing quality. At the same time, it was observed that the roughness of workpiece decreased with the increase in the cutting distance of AT10B@5 tool to 3500 m and then continued to increase slowly. This is because with the increase in cutting distance, a large amount of cutting heat was generated on the tool surface. This led to the oxidation reaction of TiB_2 in the matrix, generating a large amount of molten B_2O_3 and TiO_2 with lubrication effect and thus increasing the lubrication performance of the tool and improving the workpiece surface processing quality.

Figure 2 shows the changes between the cutting distance S and (a) wear amount of tool surface VB and (b) workpiece surface roughness Ra when AT10B@5 and AT tools cut the workpiece 40Cr hardened steel at different feeding rates (v = 300 m/min, a_p = 0.2 mm).

Figure 2 (a) shows that with the increase in feed, the cutting performance of the two tools decreased due to the increased cutting resistance between the tool and workpiece due to a larger cutting feed, leading to severe tool wear. By comparing AT and AT10B@5 tools, it was found that the effective cutting distance of AT tool was 5500 m when the feed speed was 0.102 mm/r. The cutting distance of AT10B@5 tool was greater than 6000 m with a long service life. When the feed rate increased to 0.198 mm/r, with the increase in cutting distance, the wear of the two tools became severe. The effective cutting distance was less than 5000 m, and the wear of back tool face reached 0.3 mm, satisfying the failure standard of the tool.

Figure 2 (b) shows that with the increase in the cutting feed of the two tools, the machining surface roughness of the workpiece increased, thus reducing the machining quality. By comparing the workpiece processed by AT and AT10B@5 tools, it was found that under the same cutting conditions, the AT tool had a higher machining surface roughness, and the roughness increased rapidly when the feed rate was 0.198. This is because the larger the feed, the greater the cutting force of the tool in cutting the workpiece, resulting in more heat. The resulting chip did not take away the heat in time, increasing the tool temperature and aggravating the tool damage. With the addition of h-BN@Al_2O_3, the surface roughness of AT10B@5 tool material decreased. With the increase in cutting distance, the roughness changed slightly, and a stable workpiece machining surface quality was maintained.

Figure 3 shows the changes between the cutting distance S and (a) wear amount of tool surface VB and (b) workpiece surface roughness Ra when AT10B@5 and AT tools cut the workpiece 40Cr hardened steel at different cutting speeds (v = 300 m/min, f = 0.102 mm/r).

Figure 3 shows that with the increase in the amount of cutting back, the wear degree of back surface of the two tools increased, making them more prone to failure. This is mainly because the back cutting of the tool-workpiece-machine tool system increased the vibration. At the same time, because the tool's main cutting edge and workpiece material contacted sidewise, the cutting force increased; a lot of cutting

heat was generated; and the surface temperature of the tool increased, thus decreasing the wear resistance of the tool. By comparing the curves of the two tools AT10B@5 and AT in Fig. 3 (a) with the same cutting amount on the back, it was observed that when the depth of cut was 0.1 mm, the effective cutting distance of the two tool materials AT10B@5 and AT was more than 6000 m, and the wear amount of back tool surface VB did not reach 0.3. When the depth of cut was 0.2 mm, the effective cutting distance of AT tool was about 5500 m, and the cutting distance of AT10B@5 tool material was more than 6000 m. Its wear resistance is stronger than AT tool.

Figure 3 (b) shows that both AT10B@5 and AT tools wear faster with the increase in back bite during cutting, seriously affecting the surface quality of processed workpiece. When the depth of cut was 0.1 mm and 0.2 mm, the surface roughness of the workpiece processed by AT tool had a small difference with the increase in cutting distance, exhibiting a trend of slow growth. As the depth of cut increased to 0.3 mm, the roughness of workpiece increased substantially, especially when the cutting distance increased to 4000 m, the roughness increased sharply, because the wear of the tool back face reached 0.3. However, under the same cutting conditions, the surface roughness of workpiece processed by AT10B@5 tool changed slightly with the increase in back cutting amount. When the depth of cut was 0.3 mm, the maximum surface roughness within the effective cutting distance was maintained within 1, and the surface machining quality was good.

The main parameters of 40 Cr hardened steel including the cutting speed (v), feed rate (f), depth of cut (ap) of cutting tools, surface roughness of machining workpiece, and surface wear were studied. The results show that under the same cutting conditions, the cutting tools exhibited serious wear and tear with the increase in cutting distance, and the service life of the cutter decreased. The surface roughness of workpiece increased sharply with the increase in cutting distance, severely reducing the machined surface quality. The surface wear of AT10B@5 tool increased with the increase in cutting distance, and its effective cutting distance was longer than AT tool with a longer cutting life. The workpiece surface roughness was small and maintained within 1 with stable processing quality, satisfying the needs of finishing and semifinishing. Cutting force is the force when the tool deforms the workpiece surface and produces chips during the cutting. The cutting force is mainly composed of the main cutting force (circumferential force Fz), depth of cut resistance (radial force Fx), and feed force (axial force Fy). The cutting force can be used to calculate the cutting power and analyze the stable state of the cutting tool. It is also an important basis to analyze the workpiece surface quality, cutting temperature, tool friction coefficient, and wear amount during cutting.

Figure 4 shows a cutting force comparison diagram of different tools under v = 300 m/min, a_p = 0.2 mm, and f = 0.102 mm/r. The main cutting force Fz, radial force Fy, and axial force Fx of AT10B@5 tool were all less than those of the AT tool, in which the main cutting force decreased by 20.8%. This is because the addition of a solid lubricant made the cutting system of the tool more stable, and the impact force of the tool tip decreased, thus decreasing the amount of main cutting force. According to the main cutting force Fz and radial force Fy measured during the cutting of the tool, the friction coefficient of front tool face can be calculated using Eq. 1.

$$\mu = tan(\gamma_0 + arctan(\frac{F_y}{F_z}))$$

1

where μ is the friction coefficient of the tool front face, and$\gamma_0$is the tool front angle.

Using Eq. (1), the friction coefficient of AT tool's front face was determined as 0.6, and that of AT10B@5 tool's front face was determined as 0.53, which was reduced by 11.6%. Under the same cutting conditions, the AT10B@5 tool has a lower cutting force and friction coefficient of front tool surface, thus effectively reducing the damage of the tool during the cutting and prolonging the service life of the tool.

Analysis of tool wear patterns

Figure 5 and Fig. 6 shows the micromorphology of front tool surface wear of different tool materials. Figure 5 shows a semicircular peeling area on the front cutter surface, forming a crescent sag wear morphology. It can be seen from Figure. 5 (a) - (d) of wear mechanism. Because the cutting temperature is too high, a sharp diffusion between the front tool surface and chip with a high temperature deteriorated the front tool surface performance. This made it easier for chips to remove the components of front blade. Therefore, more bond wear and some abrasive wear were observed on the front tool surface. At the same time, a micro collapse occurred at the tool tip, which was caused by a larger cutting impact force. As shown in Fig. 6, the front face of AT10B@5 tool wears evenly and smoothly with good wear resistance, and no obvious breakage was found. It can be seen from Figure. 6 (a) ~ (d) of lubrication mechanism of AT10B@5 ceramic material. This is owing to the precipitation of solid lubricant during the cutting, decreasing the friction between the chip and front cutter surface; good lubrication performance accelerated the discharge of cutting and decreased the cutting temperature. The repair agent repaired the microcrack timely and improved the reliability of the tool. Figure 6 shows that the main wear of AT10B@5 tool is bond wear.

Figures 7–11 show that AT10B@5 ceramic tool has a higher cutting life and processing quality.

According to the surface machining quality and back-tool surface wear of different tools shown in Fig. 7, AT10B@5 has better surface machining quality and tool life. Figure 8 shows the temperature test when the cutting distance reached 1000 m during the cutting test. At this time, the cutting was relatively stable, and a stable temperature distribution could be obtained. By comparing the cutting temperatures of AT and AT10B@5 tools in Fig. 8, it was found that the cutting temperature of AT10B@5 tools with TiB_2 and h-BN@Al_2O_3 was 22.2% lower than that of conventional AT tools. This is because the addition of a solid lubricant formed a lubricating film on the workpiece surface, and TiB_2 increased the lubrication performance under the cutting heat oxidation of B_2O_3 and TiO_2, thus decreasing the friction during the cutting. The lubricant made the tool chip more smooth, reduced the attachment of chip on the surface of the tool, thus removing a lot of heat and avoiding chip tumors and other adverse phenomena. A decrease in cutting temperature is beneficial to improve the surface quality of workpiece, reduce tool wear, and enhance the service life of the tool.

Figures 9 and 10 show that mechanical furrow scratches appeared in both tools in the wear area of rear cutter face. Figure 9 clearly shows the scratches in AT tool; a lot of deep scratches and damage zone appeared on the knife surface. It can be seen from Figures. 9 (a) (b) of wear mechanism. This is mainly because long scratches were formed during the cutting of artifacts with hard particles on the surface of cutter knife. When scratches were accumulated substantially, under the action of cutting force, cutting temperature and diffusion made the blade fall off, thus forming a narrow broken belt. This is a typical abrasive wear morphology. As shown in the region magnification Fig. 9, under a large amount of cutting heat, the tool back surface has partial bonding. Thus, bonding wear was formed.

Figure 10 shows that the overall wear area and wear depth of AT10B@5 tool back surface are relatively small, and no obvious edge collapse occurred. Figure 10 (a)-(c) is the schematic diagram of tool repair oxidation. It can be seen intuitively that the self-repair ceramic tool has more oxidation repair process in the cutting process than the ordinary ceramic tool, and the tool can have a higher life. Analysis of and Fig. 11 shows that a large amount of H-BN precipitates in the wear area of rear tool face of AT10B@5, because of the precipitation damage of h-BN@Al_2O_3 under cutting friction, and it was uniformly dragged and covered on the friction surface to form a lubrication film. At the same time, it was observed that oxidation wear occurred on the back surface of AT10B@5 tool, because of the cutting heat generated during the cutting. TiB_2 and a part of h-BN in the tool were oxidized; amorphous B_2O_3 and TiO_2 had good crack repair effect. The microscopic morphology in Fig. 10 shows microcracks in the wear zone; the cracks are partially repaired after filling and repairing with B_2O_3 and TiO_2. These two substances have excellent lubrication effect at the same time, and they can effectively reduce the degree of knife surface wear The knife surface was also found in some areas of spalling, because bond wear occurred on the knife surface. With cutting, the adhesive on the knife surface fall off under the action of cutting shear force, removing a part of the tool and causing the damage of tool part. As can be seen from the regional magnification in Figure. 10, there are partial oxidation wear and slight abrasive wear on the wear surface.

Conclusion

In this study, the cutting performance of self-lubricating ceramic tools with repair ability was studied by adding TiB_2 and h-BN@Al_2O_3. The effects of different cutting speed (v), feed rate (f), and depth of cut (a_p) on the wear amount of tool material, surface roughness of machined workpiece, and effective cutting distance were analyzed by conducting cutting tests. The effects of the addition of TiB_2 and h-BN@Al_2O_3 on the cutting force and cutting temperature during the cutting were studied. The wear morphology of cutting tool was analyzed.

The main conclusions are as follows:

(1) The wear of AT and AT10B@5 ceramic tools increased with the increase in cutting distance, exhibiting an increasing trend with the increase in cutting speed, back bite, and feed. However, the effective cutting distance of AT10B@5 tool is longer; it can significantly improve the workpiece processing surface quality,

decrease the workpiece surface roughness with the increase in cutting speed. The overall roughness is less than 1; the degree of change is small, with stable surface processing quality.

(2) Compared with AT tool, the cutting force and cutting temperature of AT10B@5 ceramic tool material decreased significantly during the cutting. The main cutting force decreased by 20.8%; the cutting temperature decreased by 22.2%; and the friction coefficient of the front tool face decreased by 11.6%, thus effectively improving the surface quality of workpiece, reducing tool wear, and extending the service life of the tool.

(3) During cutting, the main wear of AT tool front face is bond wear, accompanied by micro edge collapse, and the main wear of back face is abrasive wear. In AT10B@5, the wear of tool front surface is bond wear, while the wear of tool back surface is shallow and relatively small. The main wear is bond wear, oxidation wear, and slight abrasive wear, among which oxidation wear is beneficial to tool crack repair.

Declarations

Competing Interest

The authors declare that they have no known competing financial interests or personal relationships that could have appeared to influence the work reported in this paper.

Author Contributions

Conceptualization, Zhaoqiang Chen; methodology, Zhaoqiang Chen, Lianggang Ji and Yuxin Shi; validation, Lianggang Ji and Yuxin Shi; formal analysis, Yuxin Shi; investigation, Zhaoqiang Chen; resources, Mingdong Yi; data curation, Yuxin Shi; writing—original draft preparation, Lianggang Ji and Yuxin Shi; writing—review and editing, Yuxin Shi and Zhaoqiang Chen; visualization, Hui Chen and Jingjie Zhang; supervision, Chonghai Xu; project administration, Chonghai Xu; funding acquisition, Zhaoqiang Chen. All authors have read and agreed to the published version of the manuscript.

Funding

This work is financially supported by the Natural Science Foundation of Shandong Province (grant number ZR2020ME155); the Shandong Province Key Research and Development Plan (grant number 2020CXGC011004); the National Natural Science Foundation of China (grant number 52075276); the Shandong Province Key Research and Development Plan (grant number 2019GGX104084); and the Project for the Innovation Team of Universities and Institutes in Jinan (grant number 2018GXRC005).

References

1. Sreejith PS, Ngoi BKA (2000) Dry machining: Machining of the future. J Mater Process Tech 101:287–291. https://doi.org/10.1016/S0924-0136(00)00445-3

2. Krolczyk GM, Maruda RW, Krolczyk JB et al (2019) Ecological trends in machining as a key factor in sustainable production – A review. J Clean Prod 218:601–615. https://doi.org/10.1016/j.jclepro.2019.02.017
3. Narutaki N, Yamane Y, Tashima S et al (1997) A New Advanced Ceramic for Dry Machining. Cirb Ann-manuf Techn 46:43–48. https://doi.org/10.1016/S0007-8506(07)60772-0
4. Huang CZ, Ai X (1996) Development of advanced composite ceramic tool material. Mater Res Bull 31:951–956. https://doi.org/10.1016/s0025-5408(96)00078-5
5. Jia L, Zhang X, Han W (2012) The hybrid effect of SiC whisker coupled with ZrO_2 fiber on microstructure and mechanical properties of ZrB_2-based ceramics. Mat Sci Eng A-Struct 551. http://dx.doi.org/10.1016/j.msea.2012.05.006
6. Deng JX, Cao TK, Liu LL (2005) Self-lubricating behaviors of Al_2O_3/TiB_2 ceramic tools in dry high-speed machining of hardened steel. J Eur Ceram Soc 25:1073–1079. https://doi.org/10.1016/j.jeurceramsoc.2004.03.033
7. He HB, Li HY, Zhang XY et al (2019) Research on the Cutting Performances and Wear Mechanisms of TiAlCrN Coated Tools During Dry Turning. Int J Precis Eng Man. https://doi.org/10.1007/s12541-019-00026-y
8. Xing YQ, Deng JX, Zhao J et al (2014) Cutting performance and wear mechanism of nanoscale and microscale textured Al_2O_3/TiC ceramic tools in dry cutting of hardened steel. Int J Refract Met H 43:46–58. http://dx.doi.org/10.1016/j.ijrmhm.2013.10.019
9. Deng JX, Cao TK, Yang XF et al (2006) Self-lubrication of sintered ceramic tools with CaF_2 additions in dry cutting. Int J Mach Tool Manu 46:957–963. https://doi.org/10.1016/j.ijmachtools.2005.07.047
10. Chen H, Xu CH, Xiao GC et al (2016) Investigation of Al_2O_3/TiC ceramic cutting tool materials with the addition of SiC-coated h-BN: preparation, mechanical properties, microstructure and wear resistance. Int J Mater Res 107:735–740. https://doi.org/10.3139/146.111395
11. Zhai WZ, Lu WL, Zhang P et al (2017) Wear-triggered self-healing behavior on the surface of nanocrystalline nickel aluminum bronze/Ti_3SiC_2 composites. Appl Surf Sci 436:1038–1049. https://doi.org/10.1016/j.apsusc.2017.12.138
12. Zhang S, Xiao GC, Chen ZQ et al (2020) Influence of $CaF_2@Al_2O_3$ on Cutting Performance and Wear Mechanism of Al_2O_3/Ti(C,N)/$CaF_2@Al_2O_3$ Self-Lubricating Ceramic Tools in Turning. Material 13:2922. https://doi.org/10.3390/ma13132922
13. Guo J (1992) The frontiers of research in ceramics science. J Solid State Chem 96:108–114. https://doi.org/10.1016/S0022-4596(05)80302-0
14. Zhao GL, Huang CZ, He N et al (2017) Fabrication and cutting performance of reactively hot-pressed TiB_2-TiC-SiC ternary cutting tool in hard turning of AISI H_{13} steel. Int J Adv Manuf Tech. https://doi.org/10.1007/s00170-016-9789-4

15. Wang RZ, Li WG (2017) Determining fracture strength and critical flaw of the ZrB_2–SiC composites on high temperature oxidation using theoretical method. Compos Part B-eng 129:198–203. https://doi.org/10.1016/j.compositesb.2017.07.065
16. Lange FF, Gupta TK (1970) Crack Healing by Heat Treatment. J Am Ceram Soc 53:54–55. https://doi.org/10.1111/j.1151-2916.1970.tb12002.x
17. Lin J, Huang Y, Zhang HA (2014) Crack healing and strengthening of SiC whisker and ZrO_2 fiber reinforced ZrB_2 ceramics. Ceram Int 40:16811–16815. http://dx.doi.org/10.1016/j.ceramint.2014.07.040
18. Li MS, Huang CZ, Zhao B et al (2017) Crack-healing behavior of Al_2O_3-TiB_2-$TiSi_2$ ceramic material. Ceram Int 44:2132–2137. http://dx.doi.org/10.1016/j.ceramint.2017.10.164
19. Huang MY, Li Z, Wu J et.al (2015) Multifunctional Alumina Composites with Toughening and Crack-Healing Features Via Incorporation of NiAl Particles. J Am Ceram Soc 98:1618–1625. https://doi.org/10.1111/jace.13508
20. Zhang WL, Yi MD, Xiao GC et al (2017) Al_2O_3-coated h-BN composite powders and as-prepared Si_3N_4 -based self-lubricating ceramic cutting tool material. Int J Refract Met H 71:1–7. https://doi.org/10.1016/j.ijrmhm.2017.10.018
21. Houjou K, Ando K, Liu SP et al (2004) Crack-healing and oxidation behavior of silicon nitride ceramics. J Eur Ceram Soc 24:2329–2338. https://doi.org/10.1016/S0955-2219(03)00645-9
22. Huy DV, Makoto N (2020) Crack-healing performance and oxidation behavior of SiC dispersed yttrium silicate composites. J Asian Ceram Soc. https://doi.org/10.1080/21870764.2020.1734153
23. Zhang XH, Xu Y, Du SY et al (2008) Preoxidation and Crack-Healing Behavior of ZrB_2–SiC Ceramic Composite. J Am Ceram Soc 91:4068–4073. https://doi.org/10.1111/j.1551-2916.2008.02760.x
24. Nguyen ST, Nakayama T, Suematsu H et al (2019) Self-healing behavior and strength recovery of ytterbium disilicate ceramic reinforced with silicon carbide nanofillers. J Eur Ceram Soc 39:3139–3152. https://doi.org/10.1016/j.jeurceramsoc.2019.03.040
25. Wang M, Wang JH, Liu X et al (2021) Preparation, corrosion resistance and self-healing behavior of Cu-MBT@HNTs/epoxy coating. React Funct Polym 160:104826. https://doi.org/10.1016/j.reactfunctpolym.2021.104826

Figures

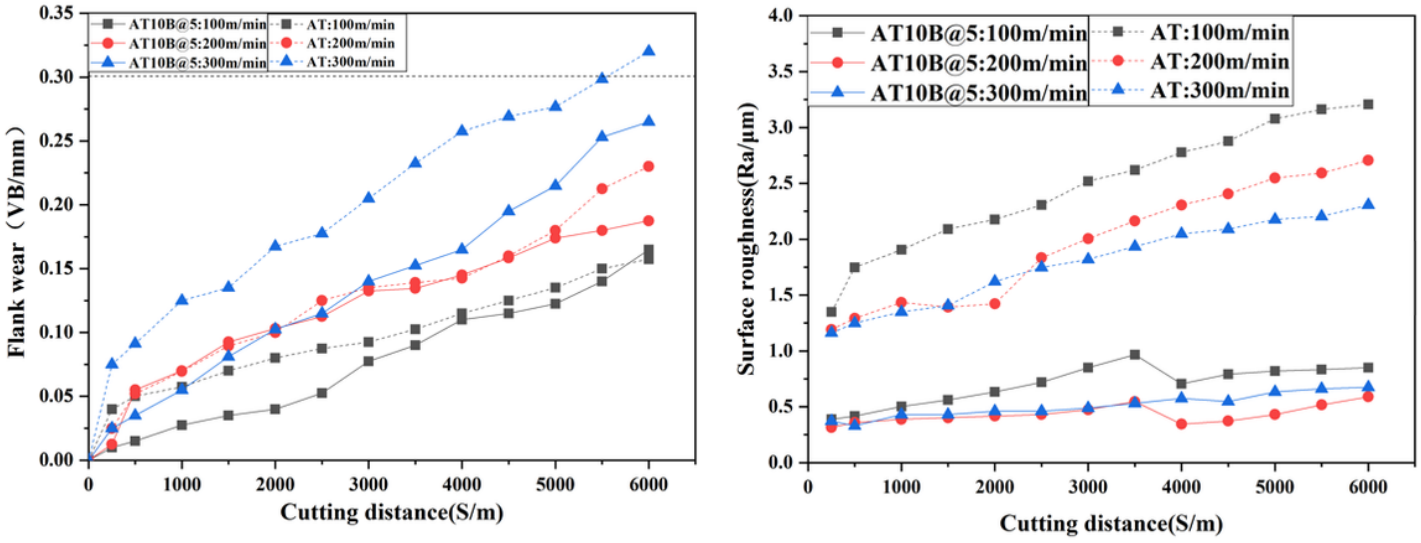

Figure 1

Wear of back tool face and surface roughness of workpiece at different cutting speeds with different tool materials (f = 0.102 mm/r, a_p = 0.2 mm)

(a) Relationship between the cutting distance and wear of back tool face of workpiece under different cutting speeds with different tool materials

(b) Relationship between workpiece surface roughness and cutting distance under different cutting speeds with different tool materials

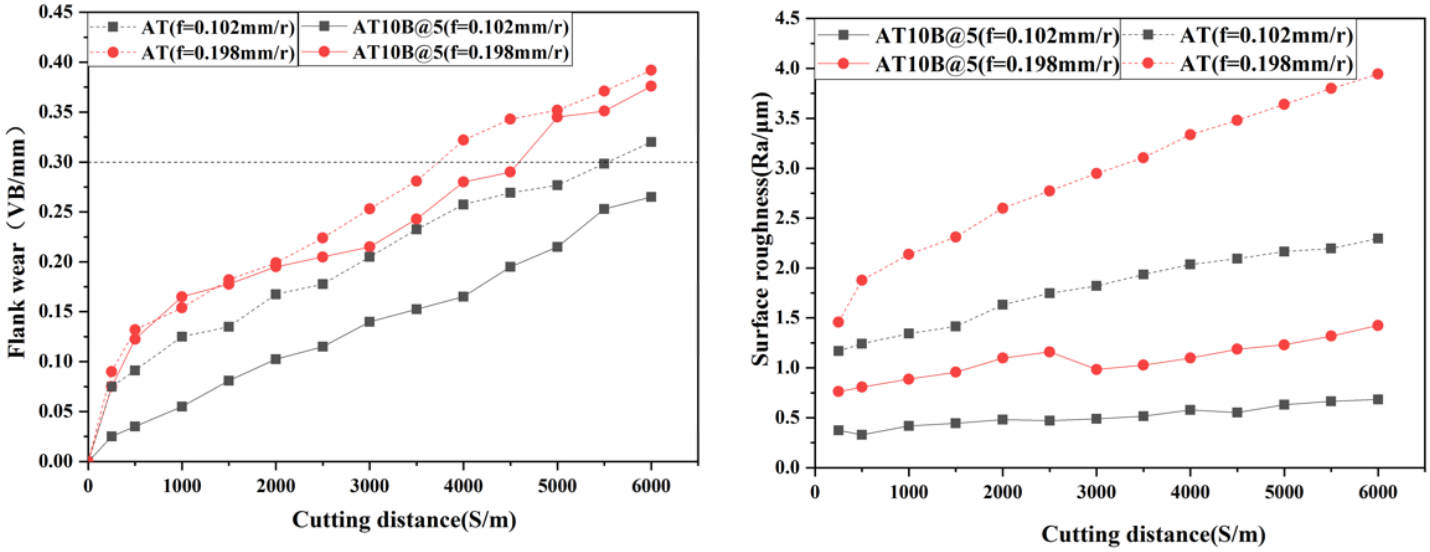

Figure 2

Rear tool surface wear and workpiece surface roughness of different tools at different feeding rates (v = 300 m/min, a_p = 0.2 mm)

(a) Relationship between the wear amount of workpiece rear tool surface and cutting distance under different cutting material feeding

(b) Relationship between workpiece surface roughness and cutting distance under different cutting material feeding

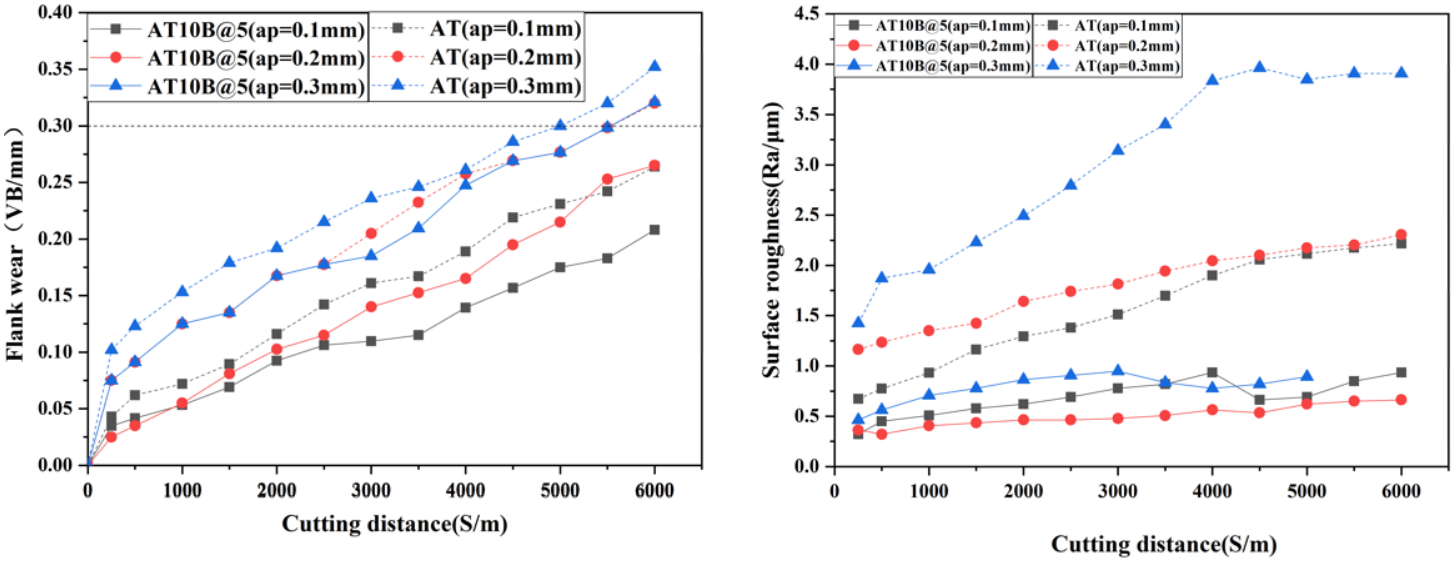

Figure 3

Rear tool surface wear and surface roughness of different tool materials under different depths of cut (v = 300 m/min, f = 0.102 mm/r)

(a) Relationship between the wear amount of workpiece's back tool surface and the cutting distance with different cutting tool materials

(b) Relationship between surface roughness and cutting distance of workpiece under different cutting tool materials and different depths of cut

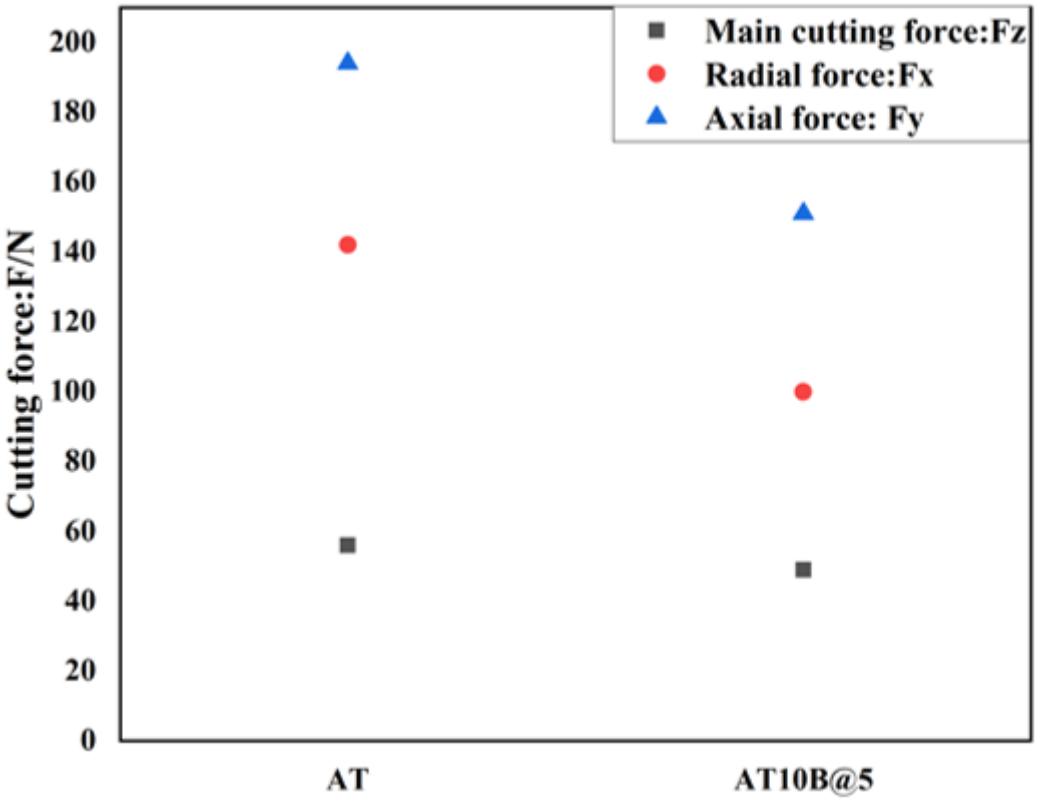

Figure 4

Comparison of cutting forces during the cutting of different tools

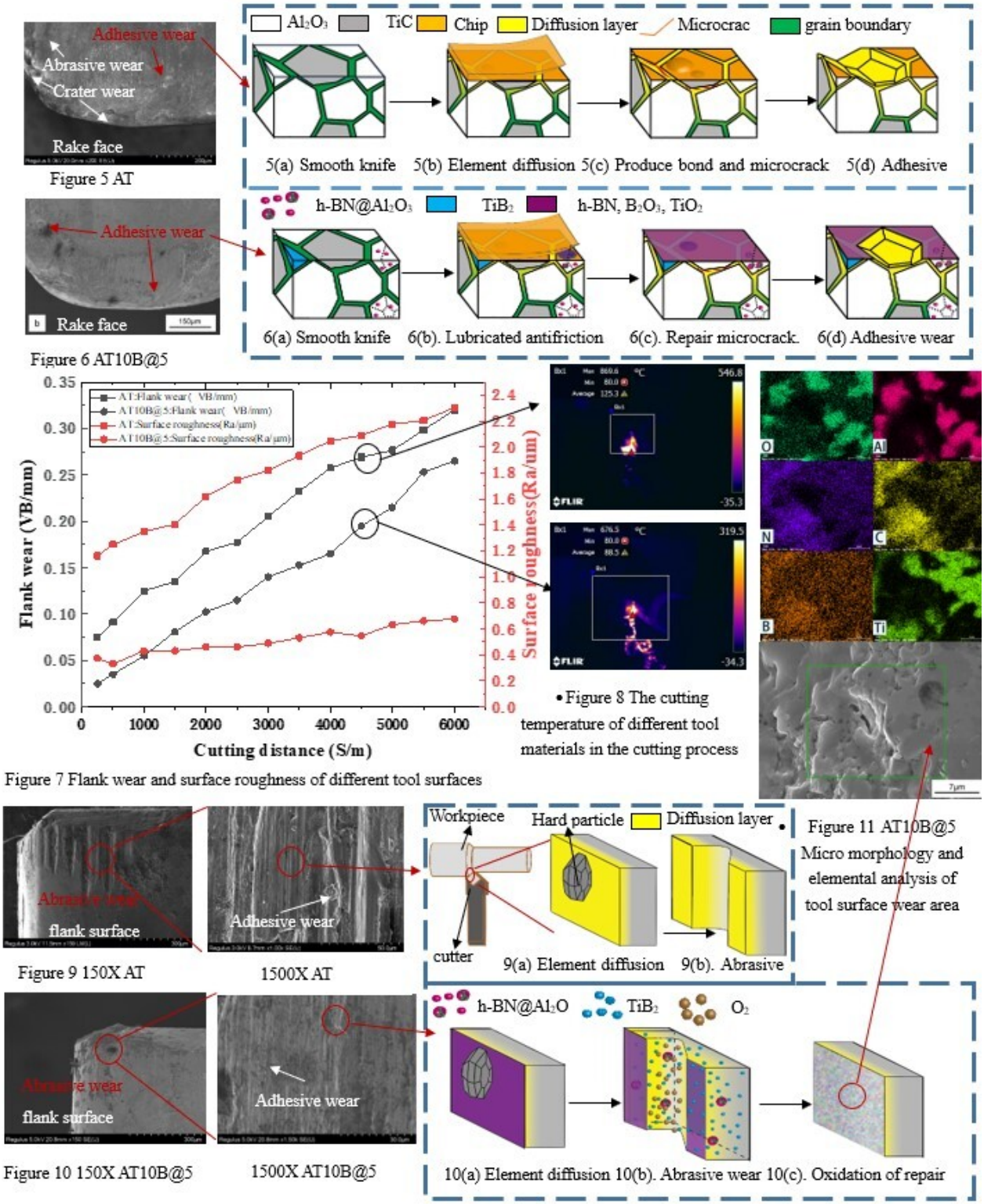

Figure 5

5-11. Lubrication mechanism diagram of tool wear and repair when cutting 40Cr hardened steel (v = 300 m/min, ap = 0.2 mm, f = 0.102 mm/r).